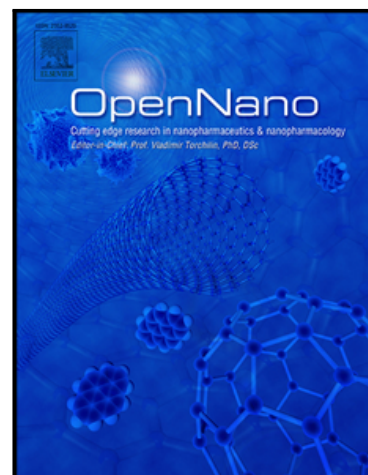# Journal Pre-proof

Instantaneous Topical Drug Quantification using a 3D Printed
Microfluidic Device and Coherent Raman Imaging

Benjamin A. Kuzma , Dandan Tu , Avery Goss , Fotis Iliopoulos ,
Julian Byrne Slade , Anna Wiatrowski , Amin Feizpour ,
Conor L. Evans

Please cite this article as: Benjamin A. Kuzma , Dandan Tu , Avery Goss , Fotis Iliopoulos ,
Julian Byrne Slade , Anna Wiatrowski , Amin Feizpour , Conor L. Evans , Instantaneous Topical
Drug Quantification using a 3D Printed Microfluidic Device and Coherent Raman Imaging, *OpenNano*
(2023), doi: https://doi.org/10.1016/j.onano.2023.100151

This is a PDF file of an article that has undergone enhancements after acceptance, such as the addition
of a cover page and metadata, and formatting for readability, but it is not yet the definitive version of
record. This version will undergo additional copyediting, typesetting and review before it is published
in its final form, but we are providing this version to give early visibility of the article. Please note that,
during the production process, errors may be discovered which could affect the content, and all legal
disclaimers that apply to the journal pertain.

Highlights

- Developed a 3D-printed applicator to monitor active pharmaceutical ingredients immediately after topical application.
- S4RS and the 3D printed applicator captures differences in exposure in frozen skin
- 3D printed applicator requires low formulation volume, is low-cost, and achieves low sample drift
- Propylene Glycol provides more rapid permeation of Rux compared to DGME

Instantaneous Topical Drug Quantification using a 3D Printed Microfluidic Device and Coherent Raman Imaging

Benjamin A. Kuzma[1,2,**], Dandan Tu[1,**], Avery Goss[1], Fotis Iliopoulos[1], Julian Byrne Slade[1], Anna Wiatrowski[1], Amin Feizpour[1], and Conor L. Evans[1,*]

[1]Wellman Center for Photomedicine, Massachusetts General Hospital, Harvard Medical School, Boston, 02114, USA

[2]Current Address: Drug Metabolism and Pharmacokinetics, Vertex Pharmaceuticals, Boston, Massachusetts

*Corresponding author

**These Authors contributed equally

Email address: evans.conor@mgh.harvard.edu (and Conor L. Evans)

Abstract

Cutaneous drug concentration quantification after topical application remains an active, yet challenging research area for topical drug development. Macroscale approaches quantify cutaneous pharmacokinetics 30 minutes to hours after application and miss rapid temporal and spatial dynamics, vital to comprehending drug disposition. We have developed a 3D-printed applicator coupled with an inverted microscope and a rapidly-tunable fiber optic laser to quantify active pharmaceutical ingredients via sparse spectral sampling stimulated Raman scattering. The 3D-printed applicator is cost-effective ($< \$0.70$/applicator) and utilizes a small formulation volume (20 μL). Ruxolitinib was formulated in two known permeation enhancers (propylene glycol and diethylene glycol monoethyl ether) that are known to display different permeation profiles to validate device capabilities. Results indicated that the applicator enabled relative-concentration monitoring immediately following drug product application. This approach has significant potential for investigating novel excipients, active pharmaceutical ingredients, and formulations to understand the permeation and biodistribution of these compounds.

Keywords: Topical drug delivery, Active pharmaceutical ingredient, Stimulated Raman scattering, 3D printing, Cutaneous pharmacokinetics

1. Introduction

In topical drug product development, an under-explored research area is how active pharmaceutical ingredients (APIs) penetrate the stratum corneum (SC) and permeate deeper into the skin. The API concentration changes over time are referred to as the pharmacokinetics (PK), which is correlated with

the *in vivo* effect (*i.e.*, pharmacodynamics). Systemically delivered drug products have well-defined PK principles, which have been investigated for over 100 years and include linear/nonlinear PK and saturation-limited absorption/clearance; with more investigation, these might carry over to cutaneous PK (cPK). While the thermodynamic activity might be the major driving force for API penetration through the SC [1, 2], what occurs inside the skin still has more questions than answers.

As the SC is the major barrier to xenobiotic skin penetration [3], it is pertinent to understand SC permeation to modulate API bioavailability. There are a multitude of methods to increase the API's tissue residence time and prolong the desired effect: the use of occlusive barriers, physical alterations to the skin barrier, as well as chemical penetration modulating agents. For example, an occluded formulation after application can provide a steady state API flux and thus higher local BA at the target site; however, this is not always practical and is commonly used to promote transdermal drug delivery for systemic distribution. Chemical penetration enhancers provide immense promise for API delivery to the local site of action as they can be incorporated into the formulation to increase both the API amount and the residence time at the site of action [4]. While the API residence time within various skin stratifications can be measured by macroscale methodologies, the effect of penetration enhancers immediately upon application is important for APIs intended for immediate local action or those in volatile formulations that have rapid skin permeation.

Two well-studied penetration enhancers are propylene glycol (PG; IUPAC name: propane-1,2-diol) and Diethylene glycol monoethyl ether (DGME; IUPAC name: 2-(2-Ethoxyethoxy)ethanol, also known commercially as Transcutol). These compounds are believed to enhance permeation by altering the solubility of APIs inside the skin and thereby increasing their partitioning while additional proposed mechanisms involve disturbance of the lipid bilayers [5]. As co-solvents, PG and DGME are known to enter the tissue and drive the API permeation as they diffuse into the skin ([6–8]); however, the impact on API disposition (distribution, metabolism, elimination) and, thereby, the pharmacological effects [9] is still not well understood.

Quantitative data are required to understand and model API penetration through the SC and permeation deeper into the skin. Unlike for systemically delivered therapeutics, blood concentrations do not accurately represent the API available at, or near, the site of action following topical application[10]. Fortunately, there has been a sizeable regulatory push to reduce the burden of topical drug product development and widen drug access to patients by validating surrogate cutaneous-based methods to assess topical bioavailability (BA) and bioequivalence (BE) [11–14]. One widely accepted approach is *in vitro* permeation testing (IVPT), which monitors API permeation through the skin over time [15]. In addition, there are also numerous modalities for *in vivo* or *in situ* estimation of cPK currently under investigation, including tape-stripping [14, 16], dermal microdialysis (dMD) [17, 18], dermal open flow microperfusion (dOFM) [19, 20], mass-spec imaging [21, 22], or the combination of these approaches [23], which can be quantified via LC-MS/MS. However, the aforementioned techniques quantify macro scale API concentrations, and while immensely beneficial compared to blood quantification to inform about target-site concentrations, there are drawbacks to each of these approaches. Some current methods are destructive, meaning they only can measure API concentration at a single time point for each site. Those techniques that allow for multi-time point measurements are relatively slow and miss API diffusion dynamics within the first 15-30 minutes of application; a clinically relevant time scale is needed to measure and understand epidermal skin permeation immediately after topical application. This is pertinent when using chemical permeation enhancers, where macroscale techniques may not have the time resolution to explain rapid (< 5 minute) changes in cPK. Finally, these methods may miss cPK heterogeneity[24–26]. Therefore, it would be beneficial to utilize an approach that can quantify APIs at the cellular level immediately following topical API application to track API permeation and localization throughout the skin stratifications.

An ideal approach would enable the cutaneous delivery of an API and be coupled to an imaging approach capable of microscale API quantification. One such delivery system that can monitor rapid changes on a small scale is microfluidic devices. Microfluidic devices have been used in drug research for screening, detection, metabolism, and evaluation of toxicity [27, 28]. However, studies using microfluidic devices for

cPK on *ex vivo* skin samples are sparse. There are several devices utilized to hold a skin sample for imaging in pharmaceutical research. Still, they have no drug inlet and cannot be coupled to methods for API tracking immediately after application [29, 30].

3D printing offers a route to create precision, custom delivery devices for cPK studies. 3D printing, also known as additive manufacturing, is capable of fabricating complex geometries, has the ability of rapid prototyping, and is time- and cost-efficient for customized design [31]. 3D printers in pharmaceutical applications are often based on vat polymerization, powder bed fusion, material extrusion, material jetting, or direct energy deposition. In particular, vat polymerization 3D printers are preferable for microfluidic designs as they can achieve high resolution in printing precise structures [32]. Importantly, the 3D-printed device can also be coupled with optical imaging devices to allow cellular-level resolution of formulation permeation at the time of application.

Raman-based approaches offer significant capabilities for measuring and quantifying APIs in skin [33–37]. However, the long acquisition times of spontaneous Raman often limit its capabilities for skin imaging and may compromise its temporal resolution. Fluorescence methods are only appropriate for the handful of naturally occurring fluorescent APIs, and the interference from endogenous fluorescent skin constituents poses significant challenges [38, 39].

Coherent Raman scatting imaging (CRI) is a chemically-selective, non-invasive optical imaging approach that can be utilized in bench-top and clinical settings and enables image acquisition with high temporal and spatial resolution for cPK quantification [40]. In CRI, the wavelengths of pulsed laser beams are adjusted such that their energy difference matches a molecular vibration of interest to allow for direct imaging and quantification of chemical species, including APIs. The two major CRI techniques are coherent anti-Stokes Raman scattering (CARS) and stimulated Raman scattering (SRS) [41–43]. SRS is capable of specifically quantifying APIs, due to its linear intensity relationship with concentration and the subcellular details of skin tissue structure to measure API permeation into specific skin cells and compartments [25, 44].

Previously, CRI investigations have been limited to molecules that either contained endogenous vibrational bands in the so-called Raman silent region (~2000-2300 cm^{-1}) or were "Raman labeled" to create such vibrations, *e.g.* via carbon-deuterium bonds. The silent region is a large span of vibrational energies over which there are few, if any, naturally arising biological vibrational bands, making API quantification relatively straightforward without the presence of background or interfering vibrations. Recently, SRS was utilized to quantify ruxolitinib from two different formulations within fresh nude mouse ear skin [25] by targeting the nitrile vibrational band. In principle, it is possible to quantify APIs via the collection of vibrational bands comprising their entire Raman spectrum. In the past, hyperspectral SRS methods were either too slow or too limiting in tuning range to capture accurate time-resolved images of API penetration within the skin. In addition, cutaneously delivered APIs are often within complex formulations, making it essential to measure the cPK of APIs and their formulation components to investigate how solvent systems influence APIs skin biodistribution [35, 45, 46].

Recently, Pence *et al*, developed an improved SRS method (termed sparse spectral samplings stimulated Raman scattering; S[4]RS) capable of simultaneously quantifying the permeation of APIs and excipients over time in an automated fashion [47]. This approach allows for the rapid, specific tuning to vibrational bands across the entire Raman spectrum, including the fingerprint, silent, and high wavenumber regions. By tuning into specific molecular vibrations of the APIs, excipients, and skin, the cPK of the API and excipients could be simultaneously and independently measured and co-registered with the skin's cellular structure. The recently developed S[4]RS methodology is a significant improvement for API quantification at the time of application, which has not been investigated to date. While only a proof of concept, this set the stage to investigate API permeation from complex formulations and whether inactive ingredients may influence the biodistribution of APIs.

The goals of this study were to 1) develop a 3D printed microfluidic device coupled to SRS imaging that would allow for concentration quantification at the time of API application and 2) validate the 3D printed

4

device with two commonly used permeation enhancers (PG and DGME) using the S^4RS methodology. Ruxolitinib (Rux), a selective Janus kinase (JAK) inhibitor being investigated for its use in treating skin inflammation, was used as the model API [48]. This compound contains a nitrile functional group, which enables CRI by targeting the vibrational frequency ($\sim 2{,}250$ cm^{-1}) of the Raman spectrum devoid of chemical interference from the skin. The development of this device can support a new regime of studies into drug penetration and topical formulation efficacy from the time of application.

2. Materials and Methods

2.1. Materials

Ruxolitinib (Rux) was provided by LEO Pharma (Ballerup, Denmark). 1,2-Propanediol (Propylene Glycol - PG) and Diethylene glycol monoethyl ether (DGME) were obtained from Sigma-Aldrich (Saint Louis, MO, USA). Standard clear resin was purchased from Formlabs (Somerville, MA), 25 mm diameter size 0 coverslips were purchased from Chemglass (Vineland, NJ), and UV curable optical glue (Loctite AA3321) was purchased from Henkel Loctite (Rock Hill, CT). A 25 μL syringe was used to deliver the formulation (Hamilton Syringes, Reno, NV).

2.2. General Applicator Design and Construction

The applicators were designed to minimize the formulation volume required to flow under the tissue sample. These applicators mate to standard luer press-fit syringes for easy application and volumetric control of the formulation delivered into the system. The outer walls mate to microscope incubation chambers allowing for extended time course measurements to be performed and eliminating device movement in the X, Y, and Z directions. The tissue rests on two spacers with a thickness of 100 μm to allow the formulation to flow under the tissue and contact the epidermis. These two spacers reduce the formulation volume required to fill the imaging field of view and control the formulation flow.

Applicators were built in-house using a Formlabs 3B SLA printing system with the standard clear photo-polymer resin. Printing conditions include an accuracy of 25 μm layer height with full raft supports. Print orientation was configured, so applicator channels are perpendicular to the build plate. Printed structures were then washed twice in 100% isopropyl alcohol (IPA). The support material was removed, and structures were sanded to remove any leftover support material or defects. A visual check was performed to ensure that the coverslip was completely flush with spacer planes and then UV cross-linked to the applicator bottom plane utilizing 302 nm light and maximum power settings (999,999 μJ/cm^2) for three cycles.

2.3. Sample Preparation

Rux, the API, was dissolved in each pure inactive ingredient (100 mM) (*i.e.*, PG and DGME) [25] in 2 mL polypropylene tubes and wrapped in aluminum foil to protect from light (hereinafter referred to as formulations). Each formulation was sonicated for 10 minutes and stored at room temperature (25 °C) and used within two weeks of preparation. In addition to the formulations, a standard with 61 mg/g of Rux was used in each experiment to monitor the signal variance due to changes in the optical features of the skin tissues and the power variance of the optical system.

2.4. Tissue preparation

Nude mouse ear skin was collected following euthanasia under an institutionally approved tissue collection protocol. The ears from nude nu/nu albino mice were harvested and washed in sterile PBS buffer, then frozen at -20°C; the full tissue preparation protocol can be found in [44]. One hour before the experiment, the nude mouse ear was placed in an incubation chamber at 32°C). The nude mouse ear was removed from the

incubation chamber (Tokai Hit Co., Ltd, Shizuoka-ken, Japan) and placed on a 3D-printed applicator, so the skin was flat against the spacers. Then the applicator was placed back into the single dish insert within the incubation chamber.

2.5. SRS measurements

The S^{4}RS methodology coupled with an inverted microscope was used to collect the SRS image volumes. The automated laser/microscope configuration can rapidly switch to different wavenumbers in less than 5 ms [47], allowing for rapid, sparse, hyperspectral imaging of distinct chemical species. The targeted Raman wavenumbers were defined *a priori* by independently collecting SRS spectra of the drug, solvents, and skin. The Raman shift was first set to 2,870 cm^{-1}, to target the CH$_2$ stretching vibrational mode, imaging the skin's microscale lipid structure. Next, the Raman shift was automatically toggled to 2,250 cm^{-1} to target the nitrile stretch of Rux. Imaging was performed using a 20×0.8 NA microscope objective (UPLXAPO20X, Olympus, Tokyo, Japan). Images of 1024 pixels × 1024 pixels were acquired with a pixel dwell time of 2 μs and 3 Kalman averages per line.

During imaging, the applicator holding the sample was placed in a stage-top incubator (Tokai Hit, Shizuoka-ken, Japan) to maintain the sample temperature (32 °C). Imaging was started immediately after delivering the API formulation (20 μL) via a 25 μL syringe through the applicator's luer lock. In each experiment, there were two regions of interest (ROI). One ROI was at the ear placed on the applicator against the spacers, where XYZ volumetric images were acquired with the Z depths of 0-60 μm starting at the stratum corneum and encompassed the sebaceous glands (SG), and adipocytes (AD), as previously demonstrated [25, 41]. In the other ROI, XYZ volumetric images with the Z depths of 0-50 μm were acquired with the starting position set to the top surface of the standard Rux sample. Based on the time required to carry out sequential volumetric imaging of ROIs, the temporal resolution was approximately 4 minutes. The volumetric images at both ROIs were imaged at 2,250 cm^{-1} followed by imaging at 2,870 cm^{-1}, which repeated for 2 hours in total.

2.6. Data Processing

The volumetric images of the Rux standard sample collected at 2,250 cm^{-1} were processed using the following workflow. For one image volume per specific time point, the SRS intensities of each image were compared. The image with the maximum SRS intensity, indicating the optimal depth of focus for the standard sample, was extracted, and the SRS intensity was recorded. This process was repeated for image volumes of the standard sample at all subsequent time points. The obtained SRS intensity-time profile of the standard sample tracked the system performance independent of the API's skin permeation.

A previous methodology was used to process the volumetric images of the ROI with the ear exposed to the API formulation. [25, 47] The two general steps were to 1) implement image segmentation based on the skin's microscale lipid structure and 2) calculate API concentration-time profiles in lipid-rich and lipid-poor regions. At a time point, the one XYZ image volume collected at 2,870 cm^{-1} was used to find the skin's microscale lipid structure. SRS images at the stratum corneum (SC), sebaceous glands (SG), and adipocytes (AD) were extracted, as previously described [25, 41, 44]. Next, the matched timepoint XYZ image volumes at 2,250 cm^{-1} and 2,870 cm^{-1} were processed. The Rux images (2,250 cm^{-1}) at the corresponding Z-depths of SC, SG, and AD were extracted. The total and segmented (*i.e.* lipid-rich and lipid-poor) intensities were quantified as previously described [25, 44]. The obtained "total uptake time profile", "lipid-rich area uptake time profile", and "lipid-poor area uptake time profile" were then divided by the SRS intensity-time profile of the standard Rux sample at the corresponding timepoint, which corrected the signal variance unrelated to the API's permeation through the skin.

2.7. Data and Statistical Analysis

Noncompartmental analysis (NCA) was completed in an automated fashion in R using the library

6

NonCompart [49] for both lipid-rich and lipid-poor regions. Typical PK parameters were utilized to compare the relative exposure from both formulations: Area under the flux curve (AUC_{flux}), maximum flux (J_{max}), and time at maximum flux (t_{max}). Statistical comparison of PK parameters was conducted on the natural logarithm-transformed data. t_{max} values were compared using a Wilcoxon Rank Sum test. Significance was determined to be statistically different when $p < 0.05$.

3. Results and Discussion

Determining cPK after the topical application of drug products is an expanding research area. The recent application of cutaneous-based approaches to assess local bioavailability (namely IVPT, dMD, and dOFM) has led to significant progress in the field. However, these techniques miss microscale changes, which may be important for the target-site activity and, thus, therapeutic success. Previous methods of CRI for cPK have been limited in their ability to capture early dynamics following topical application of formulations due to the experimental complexity (*i.e.*, the time between formulation application and the start of imaging). To overcome this challenge, this work sought to develop and test a new formulation applicator to directly visualize and quantify early time points of cPK.

3.1. Preliminary Applicator Design
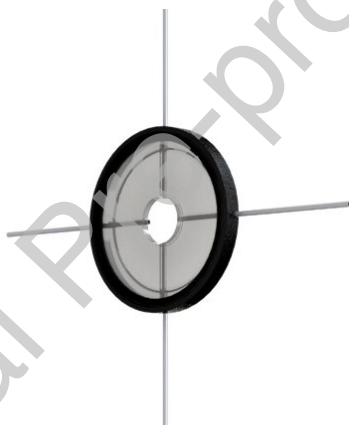
Figure 1: The first iteration of drug applicator prototype. Challenges with tissue and device movement required further improvement

Developing a low-cost applicator that could be integrated into an SRS setup was challenging. The first prototype (Figure 1) attempted to deliver the formulation through polypropylene tubing into the optically clear glass on the inverted microscope so that the formulation was in contact with the skin. Using this design, images could be collected at the time of drug application. However, the spacer height to hold the sample was large (1.25 mm), which required a large formulation volume. In addition, the spacer height led to tissue movement during API delivery, which caused significant challenges in tracking the skin tissue and the permeation of the API within the skin.

A second iteration (Figure 2A) reduced the spacer height to 250 μm to better hold the skin sample. In addition, the design consumed fewer printing materials and required a shorter printing time. Iterations No.1 and No.2 used a syringe to deliver the formulation through the polypropylene tubing (Figure 2B). This led to a relatively large "dead space" within the tubing as the tubes were several millimeters long. While the overall tissue movement was lower in the second design, injection of the formulation in the lateral direction caused physical device movement in the axial direction, which drove the sample outside the microscope focus. The challenges presented by the physical device movement and tissue movement also posed issues for accurate cutaneous API concentration quantification.
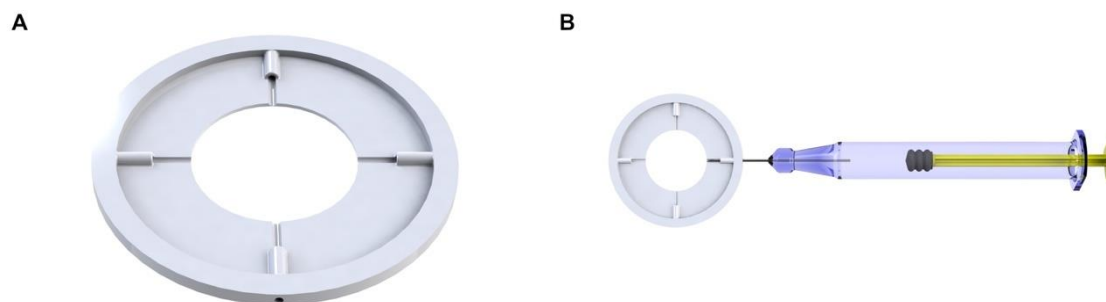
Figure 2: The second iteration of 3D applicator prototype. Physical device movement was reduced from the first prototype, but the tissue movement on the Z-axis remained too large for imaging the tissue layers of interest.

As the first several prototypes fell short due to their physical device movement, tissue movement after the formulation was applied, and the high formulation volume requirement, the first challenge was to address the physical device movement, to allow accurate imaging. The easiest solution to remove any physical device movement was to design the applicator to fit directly into the microscope dish holder, as seen in Iteration No.3 (Figure 3).

Once the physical device movement had been solved, the next challenge was the reduction in tissue movement. While the movement of 100 μm does not necessarily seem large, image volumes acquired here are 60 μm thick - smaller than the total axial drift observed in earlier designs. Though it is, in principle, possible to address this by scanning over larger axial distances at high Z-axis resolution, this requires a longer time, leading to a reduced temporal resolution in cPK measurements. It may not be possible to eliminate tissue movement completely, but this work was able to reduce axial drift to a low enough value that volumetric imaging and Z-tracking could follow the same stratifications over time.

Furthermore, the 100 μL volume may not be large, yet is quite large when considered in the context of drug development [50]. In new drug development, thousands of molecules are discovered, but ultimately only a few reach an Investigational New Drug Application submission for regulatory approval [51]. Even in the generic drug development space, developing a new topical semi-solid formulation requires a quality-by-design approach that can still be costly. [12, 52]. In this way, utilizing several mg of compounds can be a costly and time-consuming prospect for many companies. By reducing the required volume several-fold, the development of this applicator device allows for minimal use of formulation in direct microscale PK imaging studies.
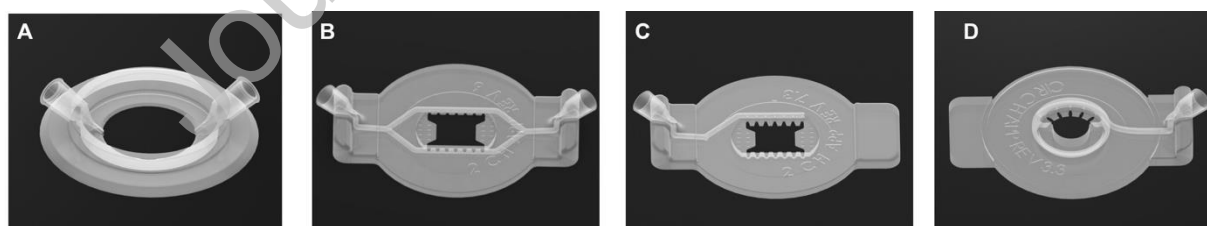
Figure 3: The progress of prototype development. A) The third iteration B) The fourth iteration C) The fifth iteration D) The sixth iteration.

Building upon these findings and desired qualities, further iterations had two main goals: 1) reduce the formulation volume required to reach the tissue and 2) reduce tissue movement for accurate imaging. Figure 3 displays the design iterations before arriving at our final applicator prototype. The details of each subsequent iteration of applicators are summarized in Table 1. Iteration No.3 removed the channels for polypropylene tubes and added sample inlets that fit a precision syringe. This design allowed the out-of-

plane injection of the formulation to eliminate lateral or vertical physical device movement. However, there was no channel guiding the formulation after injection, so the formulation could not uniformly spread out beneath the sample. In the next iteration (No.4), channels were added in the design to guide formulation flow after injection, yet due to the two branches of channels in Iteration No.4, the formulation volume to each branch was not consistent. Iteration No.5 kept one channel and displayed an improved ability to spread the formulation beneath the sample consistently. However, the design required a large formulation volume ($> 100 \ \mu$L), and significant axial direction tissue movement. In iteration No.6, the spacer height to hold the sample was further reduced to 100 μm, which decreased the required formulation volume (60 μL).
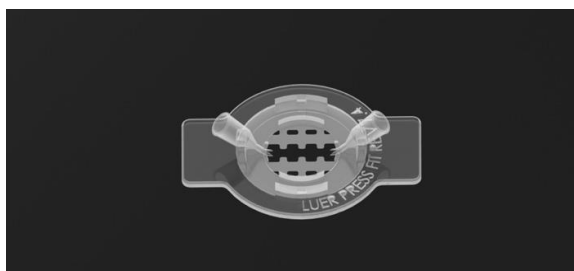
3.2. Drug applicator

The 7th generation applicator device (Figure 4) was designed to allow for the delivery of an API formulation in a controlled manner while using an inverted microscope for coherent Raman imaging studies with minimal formulation volume and tissue motion. In addition, using the inverted microscope eliminated the potential challenge of obtaining flat fields of view to quantify skin structures and API concentrations. However, an inverted geometry does result in occluded topical administration, which can drive API permeation. Occluded and unoccluded drug delivery can have a marked impact on the rate and extent of drug delivery into the skin [53, 54]. Future investigations may use an upright microscope or alternative means of supporting skin samples.

The success of this device relies on the flowability of the formulation and the ease of manufacture of the 3D-printed device. As shown in Table 1, the ability to deliver a small formulation solution volume (20 μL) is a stark improvement from previous designs that required greater than 100 μL. This improvement is due to the small spacer height to hold the sample and the removal of tubing channels. In addition, this iteration has the smallest observed drift of the tissue sample in the Z-axis among all iterations ($\leq 35 \ \mu$m). The formulation channel used a teeth-like structure to hold the skin at a constant height and allow the drug uniformly spread out beneath the sample. The 3D-printed applicator is cost-effective and has a relatively fast manufacturing time as a batch requires around 2 hours per applicator, which is much shorter compared to printing a single applicator one time. Thus, it is advantageous to print in batches due to the gain in printing time efficiency.

Table 1: Iterations of the microfluidic drug applicator. It can be seen that printing one applicator is quite time-consuming; however, printing a batch of microfluidic devices is the most time effective once a final design has been achieved.

| Iteration No.	Max Drift on the Z-axis in 30 mins (μm)	Volume of Drug (μL)	Height of the Spacer to Hold the Sample (μm)	Cost ($)	Printing Time of One Applicator	Printing Time per Batch (9 Applicators)
1	>100	>100	1250	0.41	6 h 2 min	14 h 24 min
2	>100	>100	350	0.19	5 h 20 min	9 h 25 min
3	>70	>100	500	0.60	8 h 35 min	16 h 51 min
4	40	>100	250	0.84	11 h 53 min	25 h 5 min
5	65	>100	250	0.63	9 h 28 min	16 h 50 min
6	-	60	100	0.70	9 h 39 min	17 h 59 min
7	≤ 35	20	100	0.66	10 h 36 min	18 h 25 min

9

Figure 4: Optimized microfluidic drug delivery applicator (seventh iteration). The drug formulation is delivered through the luer lock tip using a microsyringe, and the tissue lays flat on the spacers to allow imaging to take place on an inverted microscope coupled with S^4RS.

In Supplementary Movie S1, it can be seen that the formulation flows down the luer tip opening and then appears to reach the tissue-slide interface. After several more seconds, the formulation flows into the cavity between the spacers and makes contact with the tissue. The red appearance of the formulation, in this case, is due to the added food coloring that was optically clear and did not interfere with the CRI measurements of Rux.

3.3. Pharmacokinetic Analysis

The two formulations utilized are model vehicles to display the 3D printed device capabilities. PG is a known penetration enhancer that facilitates increased API, and rapid permeation compared to naive formulations [55, 56]. DGME is a known slow permeation enhancer [57] that is believed to promote API permeation due to its ability to increase drug partitioning into the stratum corneum. The PK experiments carried out here indeed indicated that Rux in PG permeated more quickly than the Rux in DGME across the skin stratifications (Figure 5).

In Figure 5A, the microscale lipid structures of the nude mouse ear skin can be observed in SRS images collected at 2,870 cm^{-1}. A machine-learning-based segmentation approach was used to automatically recognize lipid-rich from lipid-poor skin regions using the SRS contrast obtained at the CH_2 symmetric stretching vibration [25]. As shown in Figure 5B, immediately following the time of formulation application. The confidence intervals of each data point are listed in Table S1-S3 in the supplementary information. The t_{max} of the formulation with PG was observed to be earlier than that of the DGME formulation (Figure 5C). While not statistically significant in this study, the t_{max} values of the two formulations show a trend toward difference at the SC and SG layers. The J_{max} and the AUC of the two formulations were also compared (Figure 5D-E). The permeation from PG was found to be rapid. At the same time, there is a prolonged release of Rux from DGME, which aligns with previously demonstrated findings where it was demonstrated that DGME promoted cutaneous delivery of Rux over the entire experimental duration (1-hr) [25]. Indeed, if the experimental duration were extended to two hours as in this study, it would be expected that DGME would provide slow, prolonged drug delivery - as in Figure 5B.
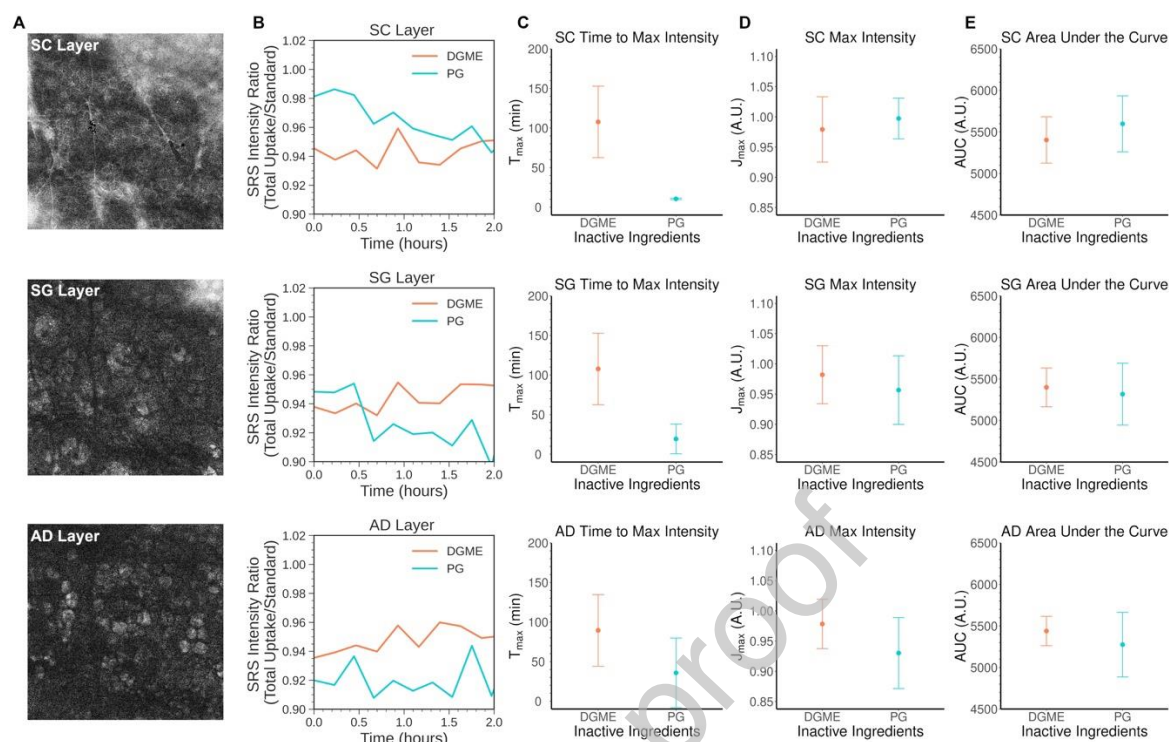
Figure 5: (A) SRS images showing the microscale lipid structures at different layers of the frozen nude mouse ear skin. Layers of the skin SC: stratum corneum, SG: layer containing the sebaceous glands, AD: layer containing the adipocytes. (B) Rux concentration-time profiles of the two formulations measured using the microfluidic drug delivery applicator. The data presented is the total API uptake (mean uptake of replicates on three ears). (C) Comparison of the t_{max} values for the layers of the two formulations. (D) Comparison of the J_{max} values for the layers of the two formulations. (E) Comparison of the AUC values for the layers of the two formulations. The results were replicates on three ears ($n = 3$) for each formulation.

The concentration-time profile in lipid-rich and lipid-poor regions are shown in Figure 6. While it can be seen that the profiles from the two formulations appear to differentiate in Figure 5 for t_{max} at the SC layer and SG layer, in the lipid-rich regions, they are similar.

When comparing the total relative concentration profiles presented in Figure 5 in the SC and the lipid-rich concentration-time profiles presented in Figure 6, it can be seen that there are t_{max} differences. These data suggest that the rapid uptake, and thus t_{max} differences, may arise from the lipid-poor regions within the SC (*i.e.*, through the corneocytes for the PG formulation). While the PG appears to promote rapid permeation (*i.e.*, t_{max}) overall, there is no difference between the maximum concentration (J_{max}) or exposure (AUC). This supports the claim, as previously suggested that PG is a rapid permeation enhancer while DGME can provide extended exposure. This is pertinent information when developing formulations and opens the possibility for future studies examining the effects and mechanisms of specific APIs, dose and exposure-dependent API and formulation effects, and potentially PK/PD relationships [45, 58]. If the goal is to provide immediate relief, this study suggests that formulations should utilize PG compared to DGME. However, if the goal is to have extended relief that does not require rapid onset, this study suggests DGME as a major excipient. Of course, topical drug products are not single solvent systems, but this approach may help design more complex drug products that are fit for purpose. While the work presented here compares the relative spatial and temporal API concentration changes, future work includes the absolute quantification of API concentrations to compare against industry gold standards, such as HPLC-UV or LC-MS/MS to further improve the applicability of this work.

11
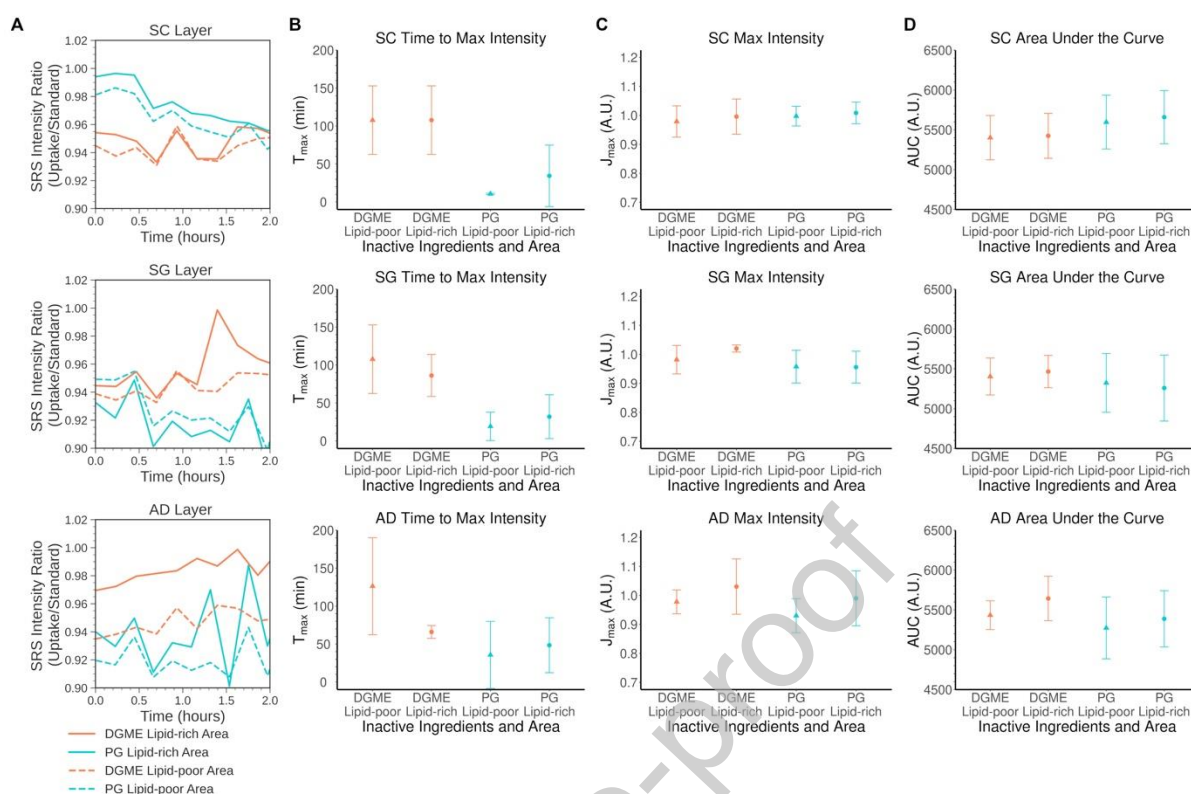
Figure 6: (A)Rux lipid-rich area and lipid-poor area concentration-time profiles measured using the microfluidic drug delivery applicator using frozen mouse ears. Layers of the skin SC: stratum corneum, SG: layer containing the sebaceous glands, AD: layer containing the adipocytes. The data presented is the uptake of API (mean uptake of replicates on three ears). (B) Comparison of the extracted tmax values, (C)Jmax values, and (D)AUC values for the layers of the lipid-rich area and lipid-poor area of the two formulations. The results were replicates on three ears (n = 3) for each formulation.

There are some limitations on the current applicator design, which could be overcome in future work to widen its application. First, the current applicator only works for low-viscosity topical drug formulation, such as solutions and lotions. To improve this, the luer tip opening connected to the channel beneath the skin should be widened for more viscous formulations, such as gels and creams. A different design would enable the application of high-viscosity formulations, such as ointments. Second, the current design achieves ≤ 35 µm drift on the Z-axis over the course of 30 mins. In this current study, frequent lipid images (one drug image volume followed by a lipid image volume) were also used to confirm the layer focused on. Pausing imaging and re-focusing were manually carried out if the layers of interest were out of the imaging range. An alternative way is to artificially scan over a larger axial range to ensure that the volume of interest remains in focus throughout the experimental time course. This leads to a somewhat restricted temporal resolution. Further improvements to the application design to reduce this remaining drift would enable less manual operation and better temporal resolution for measurements.

One of the primary goals of this device was to capture the concentrations immediately following the time of application, and many methods used today for PK studies have long, 20-30 minute gaps at the start of the study. This time gap is critical as APIs can rapidly permeate fresh skin, which currently goes uncharacterized. Even in previous CRI-based research [25], there was approximately an eight-minute gap between the initial formulation application and the beginning of imaging, due to the need for application, the skin sample positioning, and microscope setup. It is worth noting that most of the topical industry utilizes frozen skin, and there is still debate regarding how well-frozen skin accurately recapitulates fresh skin [59, 60]. If the only available tissue source is frozen skin, it would be prudent to have a device like that developed here that can deliver the formulation and quantify the drug instantaneously after application

12

with the necessary temporal and spatial resolution.

In addition to screening APIs, this 3D-printed device could be used to screen novel excipients. As demonstrated in this report, PG provides rapid permeation for Rux, and while this might not always be the case due to excipient-API interactions, novel excipients can be compared head-to-head with known penetration enhancers to understand exposure improvements. This microfluidic device only requires 20 μL of formulation, which could be utilized as an early screening tool to eliminate molecules that do not provide the desired exposure margins (brand drug development) or the desired flux profiles (generic drug development).

4. Conclusions

The 3D printed microfluidic application developed here allowed instantaneous time-point quantification of APIs and formulations in the skin using coherent Raman imaging. As this is a proof-of-concept study, further investigation into topical drug application for CRI imaging is now attainable. The combination of this device and S^{4}RS microscopy will also allow the tracking of the API and inactive ingredients at early time points, providing insight into whether inactive ingredients influence API permeation pathways and biodistribution.

References

[1] Herkenne C, Naik A, Kalia YN, Hadgraft J, Guy RH. Effect of propylene glycol on ibuprofen absorption into human skin in vivo. *Journal of pharmaceutical sciences*, 97(1):185–197, 2008.

[2] Otto A, Wiechers J, Kelly C, Hadgraft J, Du Plessis J. Effect of penetration modifiers on the dermal and transdermal delivery of drugs and cosmetic active ingredients. *Skin pharmacology and physiology*, 21(6):326–334, 2008.

[3] Jepps OG, Dancik Y, Anissimov YG, Roberts MS. Modeling the human skin barrier—towards a better understanding of dermal absorption. *Advanced drug delivery reviews*, 65(2):152–168, 2013.

[4] Williams AC, Barry BW. Penetration enhancers. *Advanced drug delivery reviews*, 64:128–137, 2012.

[5] Haftek M, Callejon S, Sandjeu Y, Padois K, Falson F, Pirot F, Portes P, Demarne F, Jannin V. Compartmentalization of the human stratum corneum by persistent tight junction-like structures. *Experimental dermatology*, 20(8):617–621, 2011.

[6] Mohammed D, Matts P, Hadgraft J, Lane M. In vitro–in vivo correlation in skin permeation. *Pharmaceutical research*, 31(2):394–400, 2014.

[7] Trottet L, Merly C, Mirza M, Hadgraft J, Davis A. Effect of finite doses of propylene glycol on enhancement of in vitro percutaneous permeation of loperamide hydrochloride. *International journal of pharmaceutics*, 274(1-2):213–219, 2004.

[8] Lane ME. Skin penetration enhancers. *International journal of pharmaceutics*, 447(1-2):12–21, 2013.

[9] Fujii M, Ohara R, Matsumi A, Ohura K, Koizumi N, Imai T, Watanabe Y. Effect of alcohol on skin permeation and metabolism of an ester-type prodrug in yucatan micropig skin. *European Journal of Pharmaceutical Sciences*, 109:280–287, 2017.

[10] Zang R, Barth A, Wong H, Marik J, Shen J, Lade J, Grove K, Durk MR, Parrott N, Rudewicz PJ, *et al.* Design and measurement of drug tissue concentration asymmetry and tissue exposure-effect (tissue pk-pd) evaluation. *Journal of Medicinal Chemistry*, 2022.

[11] Rosenberg ME, Rosenberg SP. Changes in retail prices of prescription dermatologic drugs from 2009 to 2015. *JAMA dermatology*, 152(2):158–163, 2016.

[12] Raney SG, Luke MC. A new paradigm for topical generic drug products: Impact on therapeutic access, 2020.

[13] Ghosh P, Raney SG, Luke MC. How does the food and drug administration approveapplied to topicalthe skin? generic drugs. *Food and Drug Administration's Role in Dermatology, an Issue of Dermatologic Clinics, E-Book*, 40:279–287, 2022.

[14] Raney SG, Ghosh P, Ramezanli T, Lehman PA, Franz TJ. Cutaneous pharmacokinetic approaches to compare bioavailability and/or bioequivalence for topical drug products. *Dermatologic Clinics*, 40(3):319–332, 2022.

[15] Santos LL, Swofford NJ, Santiago BG. In vitro permeation test (ivpt) for pharmacokinetic assessment of topical dermatological formulations. *Current Protocols in Pharmacology*, 91(1):e79, 2020.

[16] Imai H, Hashimoto S, Ninomiya R, Luo J, Wakuda H, Otani N, Inoue G, Amagishi H, Uemura N. Pharmacokinetics of lanoconazole in human skin after repeated topical application. *The Journal of Dermatology*, n/a(n/a):1–6, 2022.

[17] Kuzma BA, Senemar S, Ramezanli T, Ghosh P, Raney SG, Stagni G. Evaluation of local bioavailability of metronidazole from topical formulations using dermal microdialysis: Preliminary study in a yucatan mini-pig model. *European Journal of Pharmaceutical Sciences*, 159:105741, 2021.

[18] Kuzma BA, Senemar S, Ramezanli T, Ghosh P, Raney SG, Stagni G. The dose-duration effect on cutaneous pharmacokinetics of metronidazole from topical dermatological formulations in yucatan mini-pigs. *European Journal of Pharmaceutics and Biopharmaceutics*, 2022.

[19] Bodenlenz M, Tiffner KI, Raml R, Augustin T, Dragatin C, Birngruber T, Schimek D, Schwagerle G, Pieber TR, Raney SG, *et al.* Open flow microperfusion as a dermal pharmacokinetic approach to evaluate topical bioequivalence. *Clinical pharmacokinetics*, 56(1):91–98, 2017.

[20] Eirefelt S, Hummer J, Basse LH, Bertelsen M, Johansson F, Birngruber T, Sinner F, Larsen J, Nielsen SF, Lambert M. Evaluating dermal pharmacokinetics and pharmacodymanic effect of soft topical pde4 inhibitors: Open flow microperfusion and skin biopsies. *Pharmaceutical Research*, 37(12):1–12, 2020.

[21] Bonnel D, Legouffe R, Eriksson AH, Mortensen RW, Pamelard F, Stauber J, Nielsen KT. Maldi imaging facilitates new topical drug development process by determining quantitative skin distribution profiles. *Analytical and bioanalytical chemistry*, 410(11):2815–2828, 2018.

[22] Sjövall P, Skedung L, Gregoire S, Biganska O, Clément F, Luengo GS. Imaging the distribution of skin lipids and topically applied compounds in human skin using mass spectrometry. *Scientific reports*, 8(1):1–14, 2018.

[23] Handler AM, Eirefelt S, Lambert M, Johansson F, Hollesen Schefe L, Østergaard Knudsen N, Bodenlenz M, Birngruber T, Sinner F, Huss Eriksson A, *et al.* Characterizing cutaneous drug delivery using open-flow microperfusion and mass spectrometry imaging. *Molecular Pharmaceutics*, 18(8):3063–3072, 2021.

[24] Bodenlenz M, Augustin T, Birngruber T, Tiffner KI, Boulgaropoulos B, Schwingenschuh S, Raney SG, Rantou E, Sinner F. Variability of skin pharmacokinetic data: insights from a topical bioequivalence study using dermal open flow microperfusion. *Pharmaceutical Research*, 37(10):1–11, 2020.

[25] Feizpour A, Marstrand T, Bastholm L, Eirefelt S, Evans CL. Label-free quantification of pharmacokinetics in skin with stimulated raman scattering microscopy and deep learning. *Journal of Investigative Dermatology*, 141(2):395–403, 2021.

[26] Feschuk AM, Kashetsky N, Chiang C, Burli A, Burdick H, Maibach HI. Regional variation in percutaneous absorption: Evidence from in vitro human models. In *Dermal Absorption and Decontamination*, pages 235–257. Springer, 2022.

[27] Damiati S, Kompella UB, Damiati SA, Kodzius R. Microfluidic devices for drug delivery systems and drug screening. *Genes*, 9(2):103, 2018.

[28] Cui P, Wang S. Application of microfluidic chip technology in pharmaceutical analysis: A review. *Journal of pharmaceutical analysis*, 9(4):238–247, 2019.

[29] Chen X, Gr´egoire S, Formanek F, Galey JB, Rigneault H. Quantitative 3d molecular cutaneous absorption in human skin using label free nonlinear microscopy. *Journal of Controlled Release*, 200:78–86, 2015.

[30] Liu Y, Lunter DJ. Confocal raman spectroscopy at different laser wavelengths in analyzing stratum corneum and skin penetration properties of mixed pegylated emulsifier systems. *International Journal of Pharmaceutics*, 616:121561, 2022.

[31] Chen C, Mehl BT, Munshi AS, Townsend AD, Spence DM, Martin RS. 3d-printed microfluidic devices: fabrication, advantages and limitations—a mini review. *Analytical Methods*, 8(31):6005–6012, 2016.

[32] Lim SH, Kathuria H, Tan JJY, Kang L. 3d printed drug delivery and testing systems—a passing fad or the future? *Advanced drug delivery reviews*, 132:139–168, 2018.

[33] Caspers PJ, Lucassen GW, Puppels GJ. Combined in vivo confocal raman spectroscopy and confocal microscopy of human skin. *Biophysical journal*, 85(1):572–580, 2003.

[34] M´elot M, Pudney PD, Williamson AM, Caspers PJ, Van Der Pol A, Puppels GJ. Studying the effectiveness of penetration enhancers to deliver retinol through the stratum cornum by in vivo confocal raman spectroscopy. *Journal of controlled release*, 138(1):32–39, 2009.

[35] Iliopoulos F, Caspers PJ, Puppels GJ, Lane ME. Franz cell diffusion testing and quantitative confocal raman spectroscopy: In vitro-in vivo correlation. *Pharmaceutics*, 12(9):887, 2020.

[36] Iliopoulos F, Goh CF, Haque T, Rahma A, Lane ME. Dermal delivery of diclofenac sodium—in vitro and in vivo studies. *Pharmaceutics*, 14(10):2106, 2022.

[37] Jung N, Namjoshi S, Mohammed Y, Grice JE, Benson HA, Raney SG, Roberts MS, Windbergs M. Application of confocal raman microscopy for the characterization of topical semisolid formulations and their penetration into human skin ex vivo. *Pharmaceutical Research*, pages 1–14, 2022.

[38] Hermsmeier M, Jeong S, Yamamoto A, Chen X, Nagavarapu U, Evans CL, Chan KF. Characterization of human cutaneous tissue autofluorescence: implications in topical drug delivery studies with fluorescence microscopy. *Biomedical Optics Express*, 9(11):5400–5418, 2018.

[39] Jeong S, Greenfield DA, Hermsmeier M, Yamamoto A, Chen X, Chan KF, Evans CL. Time-resolved fluorescence microscopy with phasor analysis for visualizing multicomponent topical drug distribution within human skin. *Scientific reports*, 10(1):1–12, 2020.

[40] Saar BG, Contreras-Rojas LR, Xie XS, Guy RH. Imaging drug delivery to skin with stimulated raman scattering microscopy. *Molecular pharmaceutics*, 8(3):969–975, 2011.

[41] Evans CL, Potma EO, Puoris' haag M, Cˆot´e D, Lin CP, Xie XS. Chemical imaging of tissue in vivo with video-rate coherent anti-stokes raman scattering microscopy. *Proceedings of the national academy of sciences*, 102(46):16807–16812, 2005.

[42] Evans CL, Xie XS, *et al.* Coherent anti-stokes raman scattering microscopy: chemical imaging for biology and medicine. *Annual review of analytical chemistry*, 1(1):883, 2008.

[43] Pence IJ, Evans CL. Translational biophotonics with raman imaging: clinical applications and beyond. *Analyst*, 146(21):6379–6393, 2021.

[44] Kuzma BA, Pence IJ, Ho A, Evans CL. Visualizing and quantifying pharmaceutical compounds within skin using coherent raman scattering imaging. *Journal of visualized experiments: JoVE*, (177), 2021.

[45] Patel A, Iliopoulos F, Caspers PJ, Puppels GJ, Lane ME. In vitro–in vivo correlation in dermal delivery: The role of excipients. *Pharmaceutics*, 13(4):542, 2021.

[46] Mitsutake H, da Silva GHR, Breitkreitz MC, de Paula E, Bordallo HN. Neither too little nor too much: finding the ideal proportion of excipients using confocal raman and chemometrics. *European Journal of Pharmaceutics and Biopharmaceutics*, 2022.

[47] Pence IJ, Kuzma BA, Brinkmann M, Hellwig T, Evans CL. Multi-window sparse spectral sampling stimulated raman scattering microscopy. *Biomedical Optics Express*, 12(10):6095–6114, 2021.

[48] Smith P, Yao W, Shepard S, Covington M, Lee J, Lofland J, Naim A, Sheth T, Parikh B, Yeleswaram S. Developing a jak inhibitor for targeted local delivery: ruxolitinib cream. *Pharmaceutics*, 13(7):1044, 2021.

[49] Bae K. Noncompart: Noncompartmental analysis for pharmacokinetic data. r package version 0.2. 6, 2017.

[50] Hughes JP, Rees S, Kalindjian SB, Philpott KL. Principles of early drug discovery. *British journal of pharmacology*, 162(6):1239–1249, 2011.

[51] Wouters OJ, McKee M, Luyten J. Estimated research and development investment needed to bring a new medicine

to market, 2009-2018. *Jama*, 323(9):844–853, 2020.

[52] Namjoshi S, Dabbaghi M, Roberts MS, Grice JE, Mohammed Y. Quality by design: Development of the quality target product profile (qtpp) for semisolid topical products. *Pharmaceutics*, 12(3):287, 2020.

[53] Treffel P, Muret P, Muret-D'Aniello P, Coumes-Marquet S, Agache P. Effect of occlusion on in vitro percutaneous absorption of two compounds with different physicochemical properties. *Skin Pharmacology and Physiology*, 5(2):108–113, 1992.

[54] Cross SE, Roberts MS. The effect of occlusion on epidermal penetration of parabens from a commercial allergy test ointment, acetone and ethanol vehicles. *Journal of investigative dermatology*, 115(5):914–918, 2000.

[55] Carrer V, Alonso C, Pont M, Zanuy M, C´ordoba M, Espinosa S, Barba C, Oliver MA, Mart´ı M, Coderch L. Effect of propylene glycol on the skin penetration of drugs. *Archives of Dermatological Research*, 312(5):337–352, 2020.

[56] Kis N, Gunnarsson M, Berk´o S, Sparr E. The effects of glycols on molecular mobility, structure, and permeability in stratum corneum. *Journal of Controlled Release*, 343:755–764, 2022.

[57] Osborne DW, Musakhanian J. Skin penetration and permeation properties of transcutol®—neat or diluted mixtures. *Aaps Pharmscitech*, 19(8):3512–3533, 2018.

[58] Iliopoulos F, Sil BC, Moore DJ, Lucas RA, Lane ME. 3-o-ethyl-l-ascorbic acid: Characterisation and investigation of single solvent systems for delivery to the skin. *International journal of pharmaceutics: X*, 1:100025, 2019.

[59] Barbero AM, Frasch HF. Effect of frozen human epidermis storage duration and cryoprotectant on barrier function using two model compounds. *Skin pharmacology and physiology*, 29(1):31–40, 2016.

[60] Jacques-Jamin C, Duplan H, Rothe H, Vaillant O, Eilstein J, Gr´egoire S, Cubberley R, Lange D, Ellison C, Klaric M, *et al.* Comparison of the skin penetration of 3 metabolically stable chemicals using fresh and frozen human skin. *Skin pharmacology and physiology*, 30(5):234–245, 2017.

Conflicts of Interest

CLE is an inventor on patents for CARS microscopy that have been licensed to multiple microscope manufacturers. The laboratory of CLE has received sponsored research funding from pharmaceutical companies for coherent Raman imaging studies, including LEO Pharma and Pfizer.

Acknowledgements

Author Credit Statement

Benjamin A. Kuzma: Conceptualization, Methodology, Investigation, Validation, Writing- Original draft preparation.

Dandan Tu: Investigation, Validation, Formal analysis, Visualization, Writing- Original draft preparation.

Avery Goss: Conceptualization, Methodology, Visualization

Fotis Iliopoulos: Methodology, Writing- Reviewing and Editing

Julian Byrne Slade: Investigation, Visualization

Anna Wiatrowski: Investigation, Visualization

Amin Feizpour: Conceptualization

Conor L. Evans: Conceptualization, Resources, Supervision, Project administration, Funding acquisition, Writing- Reviewing and Editing
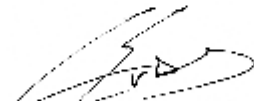
Author Agreement

Submission of work requires that the piece to be reviewed has not been previously published. Upon acceptance, the Author assigns to the OpenNano the right to publish and distribute the manuscript in part or in its entirety. The Author's name will always be included with the publication of the manuscript.

The Author has the following nonexclusive rights: (1) to use the manuscript in the Author's teaching activities; (2) to publish the manuscript, or permit its publication, as part of any book the Author may write; (3) to include the manuscript in the Author's own personal or departmental (but not institutional) database or on-line site; and (4) to license reprints of the manuscript to third persons for educational photocopying. The Author also agrees to properly credit the OpenNano as the original place of publication.

The Author hereby grants the OpenNano full and exclusive rights to the manuscript, all revisions, and the full copyright. The OpenNano rights include but are not limited to the following: (1) to reproduce, publish, sell, and distribute copies of the manuscript, selections of the manuscript, and translations and other derivative works based upon the manuscript, in print, audio-visual, electronic, or by any and all media now or hereafter known or devised; (2) to license reprints of the manuscript to third persons for educational photocopying; (3) to license others to create abstracts of the manuscript and to index the manuscript; (4) to license secondary publishers to reproduce the manuscript in print, microform, or any computer-readable form, including electronic on-line databases; and (5) to license the manuscript for document delivery. These exclusive rights run the full term of the copyright, and all renewals and extensions thereof.

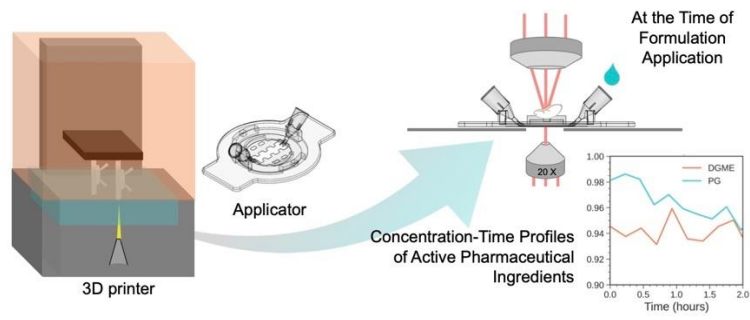I hereby accept the terms of the above Author Agreement.

Author: Conor L. Evans   2023-04-05
                                  Date:

Editor in Chief: Yan Shen   Date:

Graphical Abstract